Multivariate calibration of a water and energy balance model in the spectral domain

Valentijn R. N. Pauwels[1] and Gabriëlle J. M. De Lannoy[1]

Received 30 November 2010; revised 5 May 2011; accepted 11 May 2011; published 13 July 2011.

[1] The objective of this paper is to explore the possibility of using multiple variables in the calibration of hydrologic models in the spectral domain. A simple water and energy balance model was used, combined with observations of the energy balance and the soil moisture profile. The correlation functions of the model outputs and the observations for the different variables have been calculated after the removal of the diurnal cycle of the energy balance variables. These were transformed to the frequency domain to obtain spectral density functions, which were combined in the calibration algorithm. It has been found that it is best to use the square root of the spectral densities in the parameter estimation. Under these conditions, spectral calibration performs almost equally as well as time domain calibration using least squares differences between observed and simulated time series. Incorporation of the spectral coefficients of the cross-correlation functions did not improve the results of the calibration. Calibration on the correlation functions in the time domain led to worse model performance. When the meteorological forcing and model calibration data are not overlapping in time, spectral calibration has been shown to lead to an acceptable model performance. Overall, the results in this paper suggest that, in case of data scarcity, multivariate spectral calibration can be an attractive tool to estimate model parameters.

Citation: Pauwels, V. R. N., and G. J. M. De Lannoy (2011), Multivariate calibration of a water and energy balance model in the spectral domain, *Water Resour. Res.*, *47*, W07523, doi:10.1029/2010WR010292.

1. Introduction

[2] One of the major drawbacks in the application of physically based and conceptual hydrologic models is the requirement of accurate estimates of the various model parameters [*Duan et al.*, 1992]. Ideally, these parameters should be measured in situ, but, for a number of reasons, this approach is not possible.

[3] Remote sensing is one potential solution to this problem.

[4] However, at present a relatively large number of model parameters are impossible to estimate through remote sensing. Examples of such parameters are stomatal resistances, roughness lengths, etc. In order to overcome this problem, model parameters are frequently estimated through a comparison of the model results to observations, and a modification of the parameter values until a reasonable fit has been obtained. This methodology is commonly referred to as model calibration. A number of methods have been developed for this purpose, such as for example Bayesian recursive parameter estimation [*Thiemann et al.*, 2001], the shuffled complex evolution (SCE-UA) algorithm [*Duan et al.*, 1994; *Yapo et al.*, 1998; *Vrugt et al.*, 2003a, 2003b], the multiple start simplex (MSX) and local simplex methods [*Gan and Biftu*, 1996], simulated annealing [*Thyer et al.*, 1999], genetic algorithms [*Reed et al.*, 2000, 2003], particle swarm optimization [*Kennedy and Eberhart*, 1995], and dynamically dimensioned search [*Tolson and Shoemaker*, 2007, 2008].

[5] Although the above mentioned methods have been shown to, in many cases, lead to a good model performance, a number of problems with the automatic estimation of model parameters persist. A first problem is that physically based hydrologic models generate a large number of model outputs, while generally only one or a couple of variables are observed and used to estimate the model parameters. For this reason, a number of studies have focused on the use of multiple variables for the calibration of a hydrologic model [*Gupta et al.*, 1999; *Houser et al.*, 2001; *Crow et al.*, 2003; *Madsen*, 2003; *Scheerlinck et al.*, 2009]. Another frequently encountered problem is that reliable hydrologic models can be required in cases when calibration and validation data are scarce [*Sivapalan et al.*, 2003]. As noted by *Winsemius et al.* [2009], a general consensus has been reached that in such cases any available hydrologic information should be used to calibrate the model.

[6] In the case of scarcely gauged modeling sites, the problem may occur that model input and calibration data are not available contemporaneously [*Montanari and Toth*, 2007]. This problem can become even more relevant if multiple observations are used to estimate the model parameters, for example soil moisture profiles and evapotranspiration rates. One attractive solution to this problem is the calibration of the model in the spectral domain. In this methodology, the model parameters are adjusted in order to maximally match the Fourier coefficients of the observa-

[1]Laboratory of Hydrology and Water Management, Ghent University, Ghent, Belgium.

0043-1397/11/2010WR010292

tions and the model simulations. If the time series do not contain gaps, these coefficients can be calculated directly. If gaps in the data sets exist, the correlation function of the time series is first calculated, which is then transformed to the spectral domain. A few studies in hydrology have already applied spectral calibration, all with a focus on estimating the parameters of rainfall-runoff models using runoff observations, either through a direct Fourier transform of the time series to obtain Fourier spectra or periodograms as an approximation of the spectral density functions [*Quets et al.*, 2010], or through a Fourier transform of the correlation functions to obtain spectral density functions [*Montanari and Toth*, 2007; *Winsemius et al.*, 2009]. The objective of this paper is to assess the possibility of calibrating a physically based water and energy balance model in the spectral domain, using observations of both the soil moisture profile and the land surface energy balance.

2. Site and Data Description

[7] The data used in this study have been acquired in the framework of the AgriSAR 2006 campaign (AGRIcultural bio/geophysical retrieval from frequent repeat pass SAR and optical imaging), for which the test site was located in Mecklenburg-Vorpommern in northeast Germany, approximately 150 km north of Berlin. More specifically, time domain reflectometry (TDR) based soil moisture observations and Bowen ratio energy balance (BREB) based observations of the energy balance components in a large winter wheat field were available from 20 April through 5 July 2006, with the Bowen ratio data containing a number of gaps. The soil moisture was measured at a depth of 5, 9, 15, and 25 cm. Meteorologic data from the weather station at Görmin were available as well and can be used as model forcing from 2005 onward. All observations were converted to an hourly time step by averaging the 10 min observations. For this study, all model simulations were performed from 1 April 2006 through 5 July 2006, with an hourly time step. A detailed description of this data set is given by *Pauwels et al.* [2008].

3. Model Description

3.1. The Model Equations

[8] For the purpose of this study, the very simple water and energy balance model developed by *Scheerlinck et al.* [2009] was used. Only a short description will be provided in this section; for a full model description, we refer to *Scheerlinck et al.* [2009]. The movement of soil water in the unsaturated zone is modeled using a numerical solution to the Richards equation [*Richards*, 1931]:

$$C_m(\psi)\frac{\partial \psi}{\partial t} = \frac{\partial}{\partial z}\left(K(\psi)\frac{\partial \psi}{\partial z}\right) + \frac{\partial K(\psi)}{\partial z}, \quad (1)$$

where ψ is the pressure head (m), C_m is the specific moisture capacity (m^{-1}), t is the time (s), z is the vertical coordinate defined positive upward (m), and K is the hydraulic conductivity (m s^{-1}). The relationships between K, C_m, θ, and ψ are modeled using the Brooks-Corey equations [*Brooks and Corey*, 1964]. The parameters of these equations that need to be calibrated are the saturated hydraulic conductivity K_s (m s^{-1}), the air entry pressure head ψ_c (m), and the pore size distribution index λ (dimensionless). The saturated hydraulic conductivity is assumed to decline exponentially with depth [*Beven and Kirkby*, 1979]:

$$K_s(z) = K_s e^{-fz}, \quad (2)$$

where f is the TOPMODEL parameter (m^{-1}). Equation (1) is solved through a Crank-Nicholson finite difference discretization and a Picard iteration scheme. The boundary conditions are a Dirichlet condition (given pressure head) at the bottom of the profile (1 m depth), and a Neumann condition (given flux), calculated as the difference between the precipitation and the evapotranspiration, at the top of the profile. The evapotranspiration is calculated through an iteration for the surface skin temperature as follows [*Shuttleworth*, 1992]:

$$R_{s,i}(1-\alpha) + L_{w,i} - \epsilon\sigma T_s^4 = \frac{C_p\rho_a}{\Psi_c}\frac{e_s(T_s)-e_a}{r_{av}+r_c} + C_p\rho_a\frac{T_s-T_a}{r_{ah}} + \kappa\frac{T_s-T_1}{\triangle z}, \quad (3)$$

where $R_{s,i}$ is the incoming solar radiation (W m^{-2}), α is the surface albedo (dimensionless), $L_{w,i}$ is the incoming longwave radiation (W m^{-2}), ϵ is the emissivity (dimensionless), σ is the Stefan-Boltzmann constant (W m^{-2} K^{-4}), T_s is the surface skin temperature (K), C_p is the specific heat of moist air (J kg^{-1} K^{-1}), ρ_a is the density of air (kg m^{-3}), Ψ_c is the psychrometric constant (kg Pa^{-1}), e_s is the saturated vapor pressure (kPa), e_a is the actual vapor pressure (kPa), r_{av} is the aerodynamic resistance to vapor transport (s m^{-1}), r_c is the surface resistance (s m^{-1}), r_{ah} is the aerodynamic resistance to heat transport (s m^{-1}), T_a is air temperature (K), κ is the soil thermal conductivity (W m^{-1} K^{-1}), T_1 is the soil temperature below the first soil layer (K), which has a depth of 5 cm, and Δz is the depth of the first soil layer (0.05 m). The parameters that must be calibrated are α and κ. The left-hand side of equation (3) indicates the net radiation, the first term of the right-hand side the latent heat flux, the second term the sensible heat flux, and the third term the ground heat flux. The aerodynamic resistances for heat or vapor transport are calculated as follows [*Shuttleworth*, 1992]:

$$r_a = \frac{1}{u(z)k^2}\ln^2\left(\frac{z-d}{z_0}\right), \quad (4)$$

where $u(z)$ is the wind speed (m s^{-1}), k is the von Kármán constant ($\simeq$0.4), d is the zero plane displacement height (m), and z_0 is the roughness length for vapor or heat transport (m), depending on which aerodynamic resistance is calculated. The roughness length for vapor transport is equal to $f_v h$, with h the vegetation height (m). For heat transport this is $f_h h$. The zero plane displacement height is equal to $f_d h$. The roughness length for vapor transfer fraction f_v, the roughness length for heat transfer fraction f_h and the zero plane displacement height fraction f_d are three of the 11 parameters that must be calibrated. *Scheerlinck et al.* [2009] describes the model used for the calculation of the temporally variable vegetation height, and the relationships used between the meteorological variables and e_s, Ψ_c, and ρ_a.

[9] T_1 can be calculated through a numerical solution to the heat conduction equation:

$$\frac{\partial CT}{\partial t} = \frac{\partial}{\partial z}\left[\kappa \frac{\partial T}{\partial z}\right], \tag{5}$$

where C is the volumetric heat capacity of the soil (J m^{-3} K^{-1}), T is the soil temperature (K), and z is the vertical coordinate (m) defined positive upward with the same numbering of nodes as was used for the Richards equation. C and κ are assumed to be constant and homogeneous throughout the soil profile. Equation (5) is solved through a Crank-Nicolson finite difference discretization. The boundary conditions for this equation are a given temperature (Neumann) at both the top and bottom of the profile. At the top of the profile, this temperature is equal to T_s, and at the bottom it is equal to a predefined temperature, i.e., a linearly increasing temperature of 10°C at the beginning of the study period to 15°C at the end of the study period. These temperatures were estimated from data from nearby meteorological stations. For all applications in this study, the model is with an hourly time step, and a vertical spatial resolution of 5 cm.

[10] As a summary, 11 parameters need to be estimated: λ, ψ_c, K_s, f, α, κ, C, r_c, f_d, f_h, and f_v. All parameters are constant in time. The soil parameters are also assumed to be homogeneous throughout the profile. We acknowledge the fact that the model represents a very strong simplification of the physical reality. A state-of-the-art land surface model could have been used as well. However, this would have implied the application of a sensitivity analysis, in order to select the calibrated model parameters. This would have led to a similar amount of calibrated parameters as with this simple model. Further, the focus of the paper is on the potential of spectral calibration methods to estimate parameter values for a model that generates the required model output, not on the representation of all physical processes involved. For this reason, the model is deemed sufficiently realistic.

3.2. Coupling of the Different Processes

[11] The different equations are coupled as follows. First the energy balance equation (equation (3)) is solved. In order to solve the energy balance equation, the heat conduction equation (equation (5)) is first solved, in order to calculate T_1. This is performed iteratively, so the results of the soil heat conduction equation and the energy balance equation are consistent. The energy balance equation has as one of its results the evapotranspiration rate, which is used to calculate the soil moisture content in the top 5 cm of the soil. This is a boundary condition for the Richards equation (equation (1)), which is then solved.

4. Spectral Calibration: Definitions

[12] The idea of model calibration in the spectral domain is to adjust model parameters so the spectral properties of a simulated time series maximally match the spectral properties of an observed time series. These spectral properties can be calculated through a Fourier transform $\mathcal{F}\{x(t)\}$ of a discrete time series $x(t)$, $\forall t \in [1, D]$. More specifically, this time series can be decomposed into a number of sine and cosine waves as follows:

$$x(t) = \sum_{k=0}^{N} \Psi(k)\left[a(k)\cos\left(\frac{2\pi k}{D}(t-1)\right) + b(k)\sin\left(\frac{2\pi k}{D}(t-1)\right)\right], \tag{6}$$

where a and b are the $N+1$ Fourier coefficients $\forall k \in [0, N]$. N is equal to $D/2$ if D is an even number and equal to $(D-1)/2$ if D is an odd number. Here $b(k)$ is zero for k equal to zero. $\Psi(k) \in [\frac{1}{2}, 1,\ldots,1]$ if D is an odd number, and $\Psi(k) \in [\frac{1}{2}, 1,\ldots,\frac{1}{2}]$ if D is an even number. The amplitude of the combined wave $c(k)$ can be written as

$$c(k) = \Psi(k)\sqrt{a^2(k) + b^2(k)}. \tag{7}$$

[13] Through the Wiener-Khinchine relation the square of these Fourier coefficients is a low computational cost approximation of the spectral density function $S(k)$, as used for calibration by *Quets et al.* [2010]. In order to be able to decompose a time series into sine and cosine waves with a Fast Fourier Transform, the time series needs to be sampled with a constant time step, and no data in the time series can be missing. Especially the latter condition is frequently not met. However, the spectral density function $S_x(k)$ of a variable x is defined as the Fourier transform of the function $R_x(\tau)$ as follows:

$$S_x(k) = \mathcal{F}\{R_x(\tau)\}, R_x(\tau) = E[x(t)x(t-\tau)], \tag{8}$$

where τ is the temporal lag, and $E[\ ]$ stands for the expected value. $R_x(\tau)$ is defined as the correlation function [*Papoulis*, 1965; *Brown and Hwang*, 1992] in signal processing disciplines. Note that alternative definitions exist, with the most common other definition being the unbiased normalized correlation ($R_x(\tau)$) as defined by *Box and Jenkins* [1970], which is written as

$$R_x(\tau) = E\left[\frac{(x(t) - m_x)(x(t-\tau) - m_x)}{\sigma_x^2}\right], \tag{9}$$

where m_x and σ_x are the standard deviation and the mean of the time series, respectively.

[14] A number of remarks should be made regarding the above definitions. First, it is important to calculate the correlation function under the assumption of periodicity of the time series, meaning that the observed or modeled time series are assumed to recur regularly before the onset and after the end of the original time series. This is a basic assumption in spectral analysis.

[15] Ignoring this assumption can lead to errors in the calculation of the correlation function and consequently the spectral properties. Second, if the correlation function defined by Equation (8) is transformed, the resulting S values will be the square of the c values of the original time series. This is a consequence of the Wiener-Khinchine relation as stated above. Transformation of the unbiased normalized correlation as defined by equation (9), and multiplication of the spectral coefficients by σ_x^2, will result in the same spectral densities, except for the first harmonic, which will be zero. However, the square root of the S value of the first harmonic

as calculated by equation (8) will result in the mean of the original time series. A consequence is that, if the mean is subtracted from the time series in the calculation of the correlation function, the mean will not be calibrated. For this reason, we calculate the spectral densities using equation (8) and not using the in the hydrological sciences more widely used definition of correlation given by equation (9).

5. Time and Spectral Domain Objective Functions

5.1. Objective Function in the Time Domain for the Untransformed Time Series

[16] In automatic model calibration, an objective function is defined. The model parameters are then adjusted, until a minimum in the objective function is found. A first objective function is defined in the time domain. The model results obtained from the minimization of this objective function will serve as the baseline model calibration results, to which the results of the spectral calibration are compared. In this study eight variables (net radiation, latent, sensible, and ground heat fluxes, and soil moisture observations at four layers) are used to estimate the model parameters. Using these observations, the global objective function is defined [*Scheerlinck et al.*, 2009]:

$$\mathrm{OF}_0 = \frac{\mathrm{RMSE}_{R_n}}{\sigma_{R_n,o}} + \frac{\mathrm{RMSE}_{\mathrm{LE}}}{\sigma_{\mathrm{LE},o}} + \frac{\mathrm{RMSE}_H}{\sigma_{H,o}} + \frac{\mathrm{RMSE}_G}{\sigma_{G,o}} + \frac{\mathrm{RMSE}_{\theta_1}}{\sigma_{\theta_1,o}} + \frac{\mathrm{RMSE}_{\theta_2}}{\sigma_{\theta_2,o}} + \frac{\mathrm{RMSE}_{\theta_3}}{\sigma_{\theta_3,o}} + \frac{\mathrm{RMSE}_{\theta_4}}{\sigma_{\theta_4,o}}. \quad (10)$$

R_n is the net radiation (W m^{-2}), LE is the latent heat flux (W m^{-2}), H is the sensible heat flux (W m^{-2}), G is the ground heat flux (W m^{-2}), and θ_j is the volumetric soil moisture content of observed layer j. For each of these variables, the root-mean-square error (RMSE) is calculated as

$$\mathrm{RMSE}_x = \sqrt{\frac{1}{n}\sum_{t=1}^{n}\left[y_{o,x}(t) - y_{s,x}(t)\right]^2}, \quad (11)$$

where $y_{o,x}$ is the observed quantity and $y_{s,x}$ is the corresponding model simulation for variable x. Here n is the number of time steps with valid observations, and $\sigma_{x,o}$ is the standard deviation of the observed variable x, calculated over the calibration period.

5.2. Basic Objective Functions in the Spectral Domain

[17] As stated above, in this paper multiple variables of different magnitudes are used for the model calibration. The approach of *Scheerlinck et al.* [2009] is again used, in which for each of these variables an objective function is defined. These objective functions are then aggregated, and the resulting global objective function is minimized. In order to perform this aggregation, the objective functions for the different variables need to be of the same magnitude, to avoid the variable with the largest magnitude to excessively dominate the parameter estimation. The approach used in this paper is to normalize the coefficients of the spectral density function. This normalization is performed by simply calculating these coefficients through the Fourier transformation of the correlation function $R_x(\tau)$ divided by the variance of the observations:

$$S'_x(k) = \mathcal{F}\{R'_x(\tau)\}, R'_x(\tau) = E\left[\frac{x(t)x(t-\tau)}{\sigma^2_{x,o}}\right], \quad (12)$$

where $\sigma_{x,o}$ is the standard deviation of the observations of variable x. $R'_x(\tau)$ is defined as the normalized correlation function. It should be noted that $x(t)$ can either be a simulated or an observed time series. Both the simulated and observed correlation functions are thus divided by the observed standard deviations, in order to be consistent with the aggregation of the RMSE values in the time domain (equation (10)). $S'_x(k)$ is the spectral density function of a process with standard deviation equal to 1 for the observed time series.

[18] A similar approach as for the time domain calibration can then be applied to the decomposed normalized correlation functions. Similar to the work by *Quets et al.* [2010], a first spectral objective function is defined:

$$\mathrm{OF}'_1 = \mathrm{OF}'_{1,R_n} + \mathrm{OF}'_{1,LE} + \mathrm{OF}'_{1,H} + \mathrm{OF}'_{1,G} + \mathrm{OF}'_{1,\theta_1} + \mathrm{OF}'_{1,\theta_2} + \mathrm{OF}'_{1,\theta_3} + \mathrm{OF}'_{1,\theta_4}. \quad (13)$$

[19] $\mathrm{OF}'_{1,x}$ can be written as

$$\mathrm{OF}'_{1,x} = \sqrt{\frac{1}{N+1}\sum_{k=0}^{N}\left(\sqrt{S'_{o,x}(k)} - \sqrt{S'_{s,x}(k)}\right)^2}, \quad (14)$$

where $S'_{o,x}(k)$ is the observed spectral density for variable x and harmonic k, calculated using equation (12) and $S'_{s,x}(k)$ is the corresponding simulated spectral density. The square roots of the spectral densities $S'_x(k)$ are in fact the c values (equation (7)) of the original time series, divided by the observed standard deviation of the variable x. OF'_1 will thus focus on matching the observed and simulated Fourier amplitude spectra. The aggregation of the different spectral objective functions (equation (13)) is performed with implicit rescaling (similar to the aggregation performed in equation (10)) since the amplitudes are obtained through a transformation of $R_x(\tau)$ divided by the observed variance of the process. An equal weight is thus assigned to all the different variables. A different weight could also be assigned to the different variables, which would have the consequence that the model would perform better for some output variables than for others. Multiobjective calibration could have been performed as well, which would imply a choice of the different solutions on the Pareto front. A further examination of these possibilities is, however, outside the scope of this paper. Similar as for OF'_1, a second objective function can be defined, in which the spectral density components of the observed and simulated time series are compared:

$$\mathrm{OF}'_2 = \mathrm{OF}'_{2,R_n} + \mathrm{OF}'_{2,LE} + \mathrm{OF}'_{2,H} + \mathrm{OF}'_{2,G} + \mathrm{OF}'_{2,\theta_1} + \mathrm{OF}'_{2,\theta_2} + \mathrm{OF}'_{2,\theta_3} + \mathrm{OF}'_{2,\theta_4}. \quad (15)$$

[20] $OF'_{2,x}$ can be written as

$$OF'_{2,x} = \left[\frac{1}{N+1}\sum_{k=0}^{N}\left(S'_{o,x}(k) - S'_{s,x}(k)\right)^2\right]^{\frac{1}{4}}. \quad (16)$$

OF'_2 thus focuses on matching the observed and simulated spectral densities. For the remainder of this paper, OF'_1 and OF'_2 are referred to as the basic spectral objective functions.

[21] In this paper, only simple quadratic objective functions were thus minimized, not taking into account the characteristics of the model and observation errors. Other, more complex objective functions can also be defined, such as for example the maximization of Whittle's likelihood, which translates, for each variable x, into a minimization of the following objective function [*Montanari and Toth*, 2007]:

$$OF_{W,x} = \sum_{k=0}^{N}\left[\log\left(S_{s,x}(k) + S_{\phi,x}(k)\right) + \frac{S_{o,x}(k)}{S_{s,x}(k) + S_{\phi,x}(k)}\right]. \quad (17)$$

$S_{\phi,x}$ is the spectral density of the autoregressive function $\phi_x(B)$, with B being the backward delay operator; $\phi_x(B)$ represents the temporally variable model error. Similar to OF_1 and OF_2, $OF_{W,x}$ can be added for all variables x, leading to a single objective function OF_W, which can then be minimized. Although OF_W may be statistically more appropriate for spectral calibration than OF_1 and OF_2, it suffers from the drawback that knowledge of the characteristics of the model error is required. Although for rainfall-runoff models the assumption can be made that a first-order autoregressive model is sufficiently accurate [*Montanari and Toth*, 2007], this assumption cannot automatically be made for the model that is used in this study. Further, eight model outputs are used in this study, instead of only modeled runoff. Minimizing OF_W would thus encompass the study of the characteristics of the model error of eight variables, which falls outside the scope of this study. For this reason, the spectral analysis in this paper was limited to the use of simple, quadratic functions.

5.3. Objective Functions in the Time Domain for the Correlation Functions

[22] In order to demonstrate the benefit of transforming the correlation functions to the spectral domain, which introduces a number of extra calculations, the calibration was also performed on the correlation functions in the time domain. For each variable x, a first objective function was defined as

$$OF'_{R,x} = \sqrt{\frac{1}{N_m}\sum_{i=1}^{N_m}\left(R'_{o,x}(i) - R'_{s,x}(i)\right)^2}, \quad (18)$$

where $R'_{o,x}(i)$ is the observed value for $R'_x(i)$ (calculated using equation (12)) and $R'_{s,x}(i)$ is the corresponding simulated value. N_m is the maximum lag in the correlation function. An objective function for the calibration on the correlation functions can then be defined:

$$OF'_R = OF'_{R,R_n} + OF'_{R,LE} + OF'_{R,H} + OF'_{R,G} + OF'_{R,\theta_1} + OF'_{R,\theta_2} + OF'_{R,\theta_3} + OF'_{R,\theta_4}. \quad (19)$$

5.4. Objective Functions in the Spectral Domain Incorporating the Cross Spectra

[23] An interesting aspect of using multiple variables in the spectral domain is the fact that information on the cross correlation between variables can be used as well in the calibration. Similar to equation (12), the spectral coefficients of the cross correlation between two variables x and y can be calculated as

$$S'_{xy}(k) = \mathcal{F}\{R'_{xy}(\tau)\}, R'_{xy}(\tau) = E\left[\frac{x(t)y(t-\tau)}{\sigma_{x,o}\sigma_{y,o}}\right]. \quad (20)$$

[24] Using these spectral coefficients, an objective function can be defined, with takes into account both the correlations of the eight different variables, as well as the cross correlations:

$$OF'_{1+} = \sum_{x=1}^{8} OF'_{1,x} + \sum_{x=1}^{8}\sum_{y=x+1}^{8,y\neq x} \cdot \sqrt{\frac{1}{N+1}\sum_{k=0}^{N}\left(\sqrt{S'_{o,xy}(k)} - \sqrt{S'_{s,xy}(k)}\right)^2}, \quad (21)$$

where x and y are the calibration variables (R_n, LE, …, θ_4). Since there are eight calibration variables, there are 7 + 6 + …+ 1 = 28 cross-correlation functions. This implies that the cross correlations will have a dominating effect in OF'_{1+}. In order to ensure that both the correlations and the cross correlations have an equal weight in the calibration, a second spectral objective function is defined:

$$OF'_{1++} = \sum_{x=1}^{8} OF'_{1,x} + \frac{8}{28}\sum_{x=1}^{8}\sum_{y=x+1}^{8,y\neq x} \cdot \sqrt{\frac{1}{N+1}\sum_{k=0}^{N}\left(\sqrt{S'_{o,xy}(k)} - \sqrt{S'_{s,xy}(k)}\right)^2}. \quad (22)$$

Analogous to equation (16), the objective functions including the cross correlations can be calculated using the spectral densities, instead of the square roots thereof. These objective functions are defined as OF'_{2+} and OF'_{2++}, respectively. The objective functions which incorporate the cross-correlation properties will, for the remainder of this paper, be referred to as the extended spectral objective functions.

5.5. Important Differences Between Time and Spectral Domain Calibration

[25] As is demonstrated in section 4, the first step in spectral calibration thus consists of a calculation of the correlation functions of the different time series, which are then transformed to the spectral domain. The remark can be made that a number of different time series can all lead to the same correlation function, and thus to identical spectral properties. For example, a time series $-x(t)$ will have an identical correlation function as $x(t)$. Other examples are a time series $\pm x(t-\tau)$, with τ a temporal lag. Finally, if two time series have similar values $c(k)$ (equation (7)), they will not necessarily have the same coefficients $a(k)$ and $b(k)$ (i.e., there may be a phase shift).

[26] These possibilities, however, do not necessarily imply that good results cannot be obtained through spectral calibration. One has to realize that in this study observations of physical variables are used to calibrate a model, and that these observations are the consequence of meteorological forcings. These forcings are used by the model as well.

[27] Since the model is constructed on the basis of physical equations, uses in situ meteorological observations as forcing, and the model includes no parameters that result in only a phase shift, or the reversal of the sign of the modeled time series, it is not possible that any of the situations above will occur. Through calibration the model parameters are estimated so that the spectral properties of the observations and model similations are as similar as possible, and we will investigate under which conditions one can then make the assumption that the time series are similar.

6. Stationarity of the Time Series

[28] As explained in section 4, the correlation functions (equation (8)) of the observed and simulated time series are transformed to the spectral domain. However, the use of a temporal lag τ implies that the time series are stationary. The question can thus be raised whether or not the data used in this paper are sufficiently stationary to justify the use of equation (8) for the calculation of the spectral properties.

[29] Figure 1 shows the normalized correlation functions of all eight observed variables. In order to balance realistic lengths of this correlation function using data records of relatively short length with the requirement to use a sufficient amount of data, these correlation functions are, for the remainder of this paper, calculated with a maximal lag of one week (168 h). For the energy balance terms, a clear cyclic behavior can be noted because of the strong diurnal cycle in the data. This diurnal cycle is clearly the dominant factor in the nonstationary behavior of the energy balance time series. Figure 2 shows the corresponding values of $\sqrt{S'_{o,x}}$ and $S'_{o,x}$. For the energy balance terms, this cyclic behavior leads to a relatively high peak for the seventh harmonic, which corresponds to a wave with period 24 h ($24 \times 7 = 168$). It is possible that this harmonic will have a dominating effect in the spectral objective functions. However, Figure 1 shows that the removal of the observed average diurnal cycle from the energy balance terms, as expected, strongly reduces the cyclic behavior of the correlation functions. Figure 2 shows that this leads to spectral coefficients with values that are more similar in order of magnitude. Remaining trends do not appear in the spectral properties of the observations. It can thus be assumed, with removal of the average diurnal cycle from the energy balance observations, that the time series are sufficiently stationary to allow the use of equation (8) for the calculation of the correlation function and the spectral properties. For this reason, in the remainder of this paper, the calibration on the correlation functions in the time domain and the spectral calibration will be performed with removal of the average observed diurnal cycle from the energy balance data.

[30] In fact, this diurnal cycle is primarily a response to the external forcings, and is to a lesser extent determined by local conditions (which are represented by model parameters). Since the corresponding harmonic can dominate the spectral objective functions, the diurnal cycle can be matched with parameter values that lead to a lesser match for the other spectral coefficients. The removal of the dominant diurnal thus allows the spectral calibration to focus on the processes that are more effectively affected by the parameter choice.

7. The Parameter Estimation Algorithm: Particle Swarm Optimization

[31] The parameter estimation algorithm used in this paper, particle swarm optimization (PSO), is based on the complex, collective behavior of individuals in decentralized, self-organizing systems. These systems are created through a population of individuals that interact locally with each other and with the community. These interactions lead to global behavior, which can result in the achievement of certain objectives. Examples of such systems in nature are abundant: ant colonies, swarms of birds, schools of fish, etc. [*Kennedy and Eberhart*, 1995]. Only a short description of the method will be provided here, for a more complete description we refer to *Scheerlinck et al.* [2009].

[32] The PSO algorithm starts with the initialization of a population of N_p particles (one particle is defined as a combination of the 11 model parameters) with randomly chosen position and velocity vectors, for which the position of each particle represents a candidate solution to the optimization problem. In a D-dimensional search space the position and velocity of the ith particle, with $i = 1, \ldots, N_p$, are denoted by D-dimensional vectors $\mathbf{z}_i = (z_{i1}, z_{i2}, \ldots, z_{iD})$ and $\mathbf{v}_i = (v_{i1}, v_{i2}, \ldots, v_{iD})$, respectively. In a next step, the objective function is evaluated for each particle and is assigned a fitness function value. For each particle i a vector $\mathbf{p}_i = (p_{i1}, p_{i2}, \ldots, p_{iD})$ is defined that points to the best position that this particle has reached up to this point in the iteration cycle; it is also called the personal optimum of this particle. In other words, it is the position with the best fitness value so far in the particle's trajectory. Out of the total population, the particle that reached the best fitness function value until this point will be identified. This fitness corresponds to the solution at the position given by the vector $\mathbf{p}_g$ [*Engelbrecht*, 2003; *Clerc*, 2006]. At each iteration step, the position and velocity of each particle are updated. The global best position is memorized, and the algorithm is repeated until either a certain stopping criterion or a maximum number of iterations has been met.

[33] The PSO algorithm has only recently been introduced in hydrology, however, a number of studies have already shown that it performs well for the calibration of hydrologic models [*Gill et al.*, 2006; *Fenicia et al.*, 2008; *Castagna and Bellin*, 2009; *Tolson et al.*, 2009; *Liu and Han*, 2010; *Mousavi and Shourian*, 2010; *Zhang and Chiew*, 2010].

[34] The PSO algorithm thus depends on three parameters: c_1 (the cognitive parameter), c_2 (the social parameter), and w (the inertia weight). The convergence of the algorithm also depends on the number of particles: larger swarms need more iterations to converge. The convergence speed is not only influenced by the parameters inherent to the algorithm, but it is also influenced by the properties of the optimization problem such as the number of local optima, the position of the global optimum, the size of the search space, the objective function, and the accuracy for the determination of the posi-

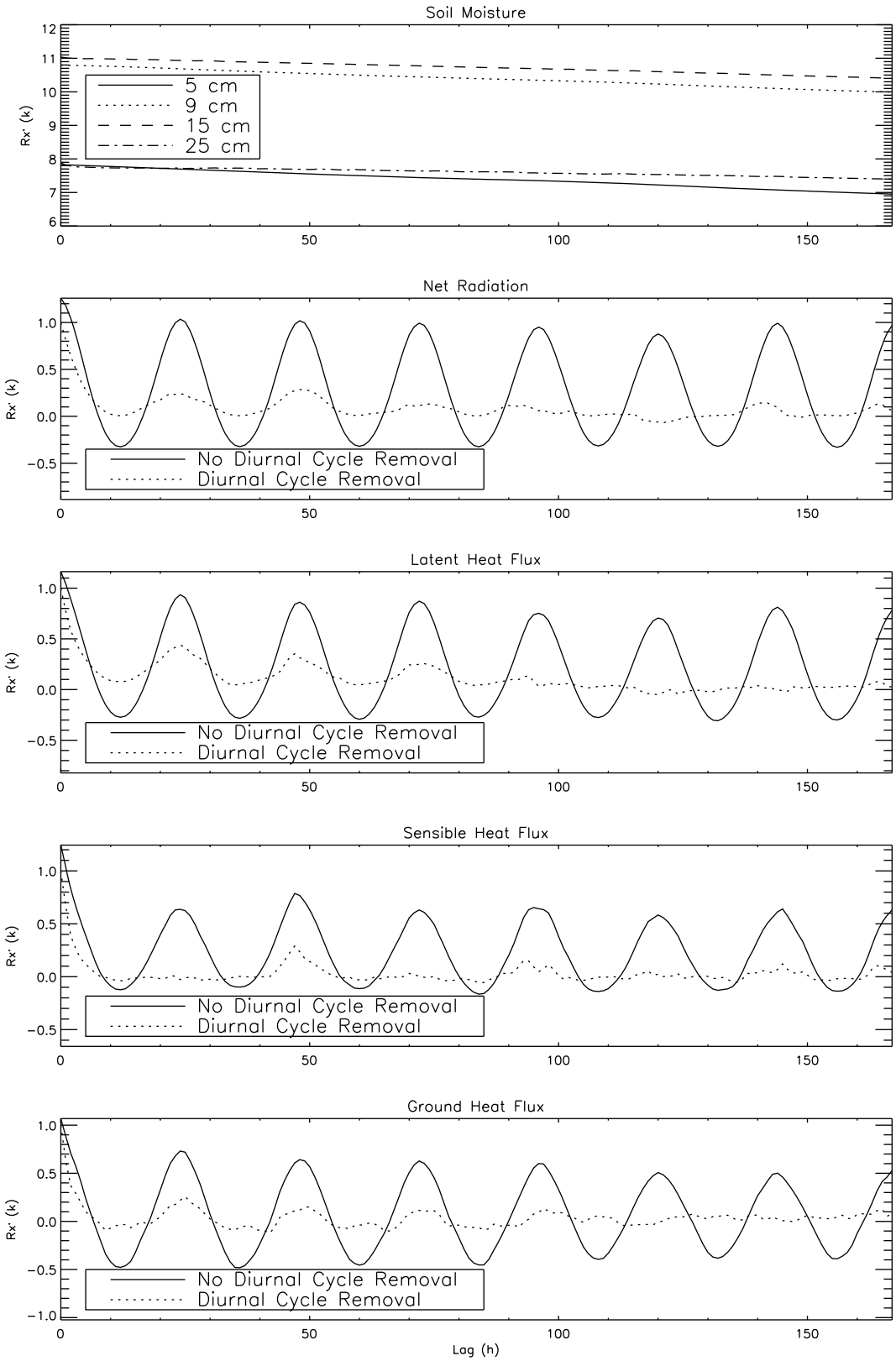

Figure 1. Normalized correlation functions for the observed variables. For the energy balance data, the functions with and without removal of the diurnal cycles are shown.

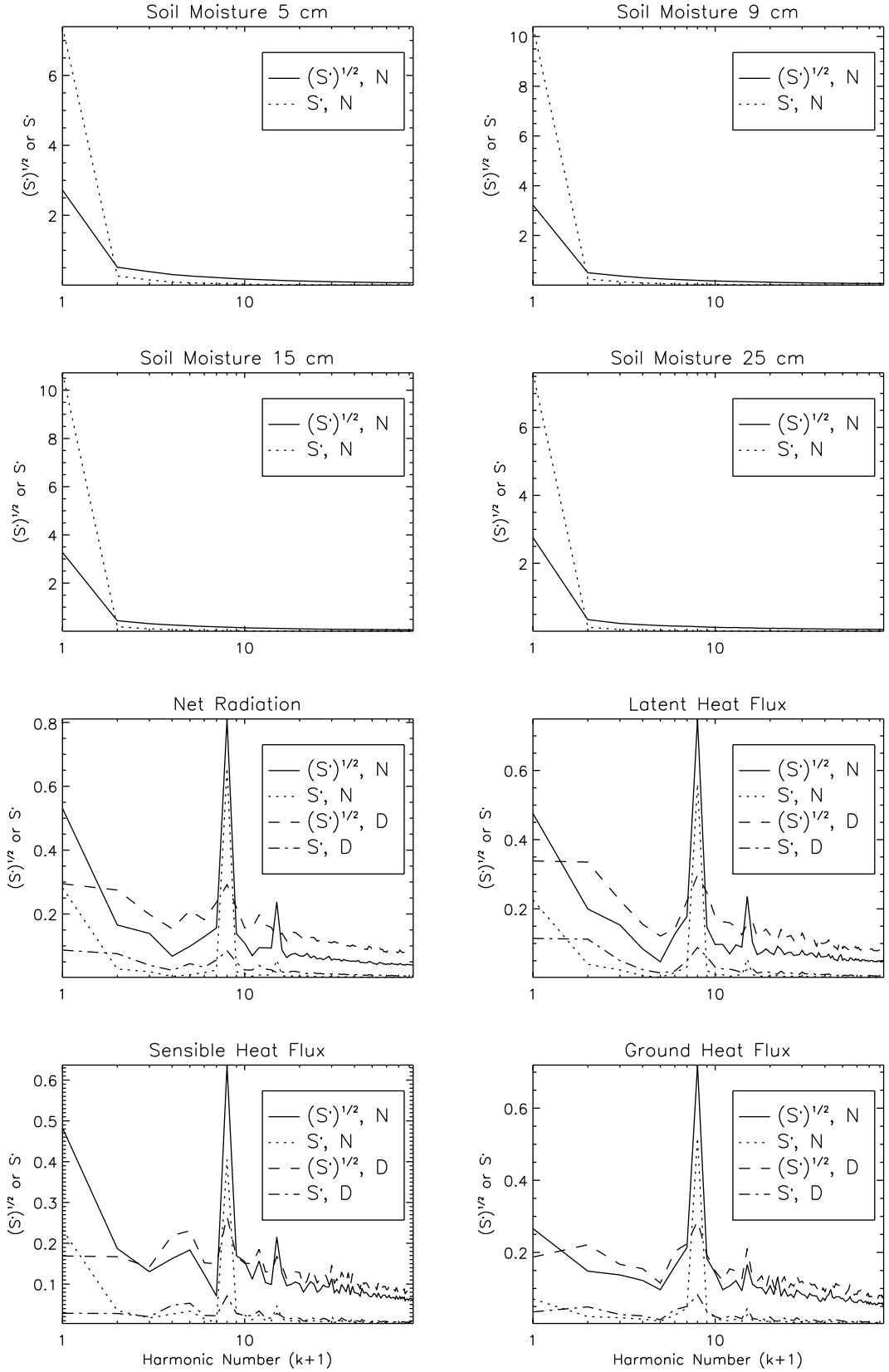

Figure 2. Values of $\sqrt{S'}$ and S' for the observed variables, with a maximum lag in the correlation function of 168 h. N stands for data without average diurnal cycle removal, and D stands for data with average diurnal cycle removal. For display reasons, $k + 1$ is the value in abscissa.

Table 1. Minimum and Maximum Values for the Different Model Parameters

Parameter	Units	Description	Minimum	Maximum
λ		Pore size distribution index	0.1	5
ψ_c	m	Bubbling pressure	−5	−0.1
K_s	m s^{-1}	Saturated hydraulic conductivity	2.78×10^{-8}	5.56×10^{-5}
f	m^{-1}	TOPMODEL exponential decay parameter	0.01	20
α		Albedo	0.01	0.9
κ	W $m^{-1}K^{-1}$	Soil thermal conductivity	0.01	5
C	J $m^{-3}K^{-1}$	Soil heat capacity	1.5×10^5	3×10^5
r_c	s m^{-1}	Surface resistance	0.01	250
f_d		Zero plane displacement height fraction	0.4	0.9
f_h		Roughness length for heat transfer fraction	0.01	0.5
f_v		Roughness length for vapor transfer fraction	0.01	0.5

tion. Hence, it is impossible to find a set of parameters that yields good results in all cases [*Engelbrecht*, 2003].

8. Implementation of the Calibration Algorithm

[35] As stated above, in the implementation of PSO, the model parameters have to be positioned in a particular parameter space. Table 1 shows the minimum and maximum values for each model parameter used in the search algorithm. When a population member is trying to move outside the parameter space during the application of the PSO algorithm, the boundaries act as perfect reflectors. In other words, the direction of displacement of that particle is inverted in order to keep it inside the parameter space.

[36] The results of PSO also depend on the choice of several parameters: the population size N_p, the cognitive parameter c_1, the social parameter c_2, and the inertia weight w. *Engelbrecht* [2003] found that a good value for the population size is $N_p = 30$. In order to determine good values for the parameters c_1, c_2, and w, an exhaustive search was performed for each objective function, with 36 iterations. The parameter c_1 was varied between 0.8 and 1.7, c_2 between 1 and 2.1, and w between 0.2 and 0.5, with steps of 0.1. The parameter values were chosen in the convergence domain of particle swarm optimization, i.e., the region for which the population will converge [*Trelea*, 2003].

9. Results: Calibration in the Time Domain

9.1. Calibration of the Untransformed Time Series

[37] In order to establish a benchmark calibration, to which the results of the spectral calibrations can be compared, the model was first calibrated in the time domain (OF_0). The PSO parameters c_1, c_2, and w, which have been determined by *Scheerlinck et al.* [2009] for this type of calibration using this model, were set to 1.5, 1.9, and 0.4, respectively. For the spectral domain calibration, the PSO parameters were determined in exactly the same manner (see section 9.2). The calibration algorithm was repeated 32 times, each time with different initial positions of the particles. Figure 3 shows the calibration result for the lowest OF_0 value. Figure 4 shows the time series of the modeled soil moisture values in detail. For this calibration, OF_0 reached a value of 3.96. For the 32 repetitions, the average OF_0 was 4.05, with a standard deviation of 0.11. Figures 3 and 4 show that, in general, and taking into account the simplicity of the model, the model simulates the soil moisture profile and the energy balance components very well. Combined with the very similar OF_0 values for the 32 repetitions, it can be assumed that these results are the best results that can be obtained for this data set with the relatively simple water and energy balance model. In the remainder of the paper, it will be assessed to what extent calibration in the spectral domain can approach these results.

9.2. Calibration of the Correlation Functions

[38] In order to find the optimal PSO parameters for the objective function for the correlation functions (OF'_R), the values for c_1, c_2 and w were varied with steps of 0.1 within the limits as described in section 8. This led to 480 ($10 \times 12 \times 4$) PSO parameter combinations. Similar to the time domain using OF_0, for each of these PSO parameter combinations the calibration algorithm was repeated 32 times, each time with different initial model parameter values, and the objective function was minimized. With the obtained model parameters, the model was applied, and the corresponding value for OF_0 was calculated for model verification.

[39] Figure 5 (top) shows the relationship between the average value for OF'_R and the corresponding average value for OF_0, for all 480 PSO parameter combinations, with 32 repetitions per PSO parameter combination. From this plot, it can be concluded that even the PSO parameter combination leading to the lowest average value for OF'_R corresponds to a relatively high value for OF_0. More specifically, calibration on the untransformed time series in the time domain led to an average value of 4.05 for OF_0, while in this case a value of 6.35 was obtained. Figure 5 (bottom) shows the relationship between the values for OF'_R and the corresponding value for OF_0, for each of the 32 repetitions of the calibration algorithm with the best PSO parameter combination. It is clear that there is a poor relationship between the values for the objective functions calculated on the correlation functions and the corresponding value for OF_0. This poor performance can be explained by the fact that calibration on the correlation function leads to a maximal fit of the values for the correlation with different lag values, as opposed to calibration on the original time series, which attempts to match the observations at every time step in the model application.

[40] Table 2 shows, for this same PSO parameter combination, the value of OF_0 corresponding to the lowest value for the correlation function objective function. The model parameter combination for which OF'_R is minimal clearly leads to a relatively poor performance in the time domain. Table 3 shows, for all objective functions, the comparison of the statistics of the linear regressions between the simulated

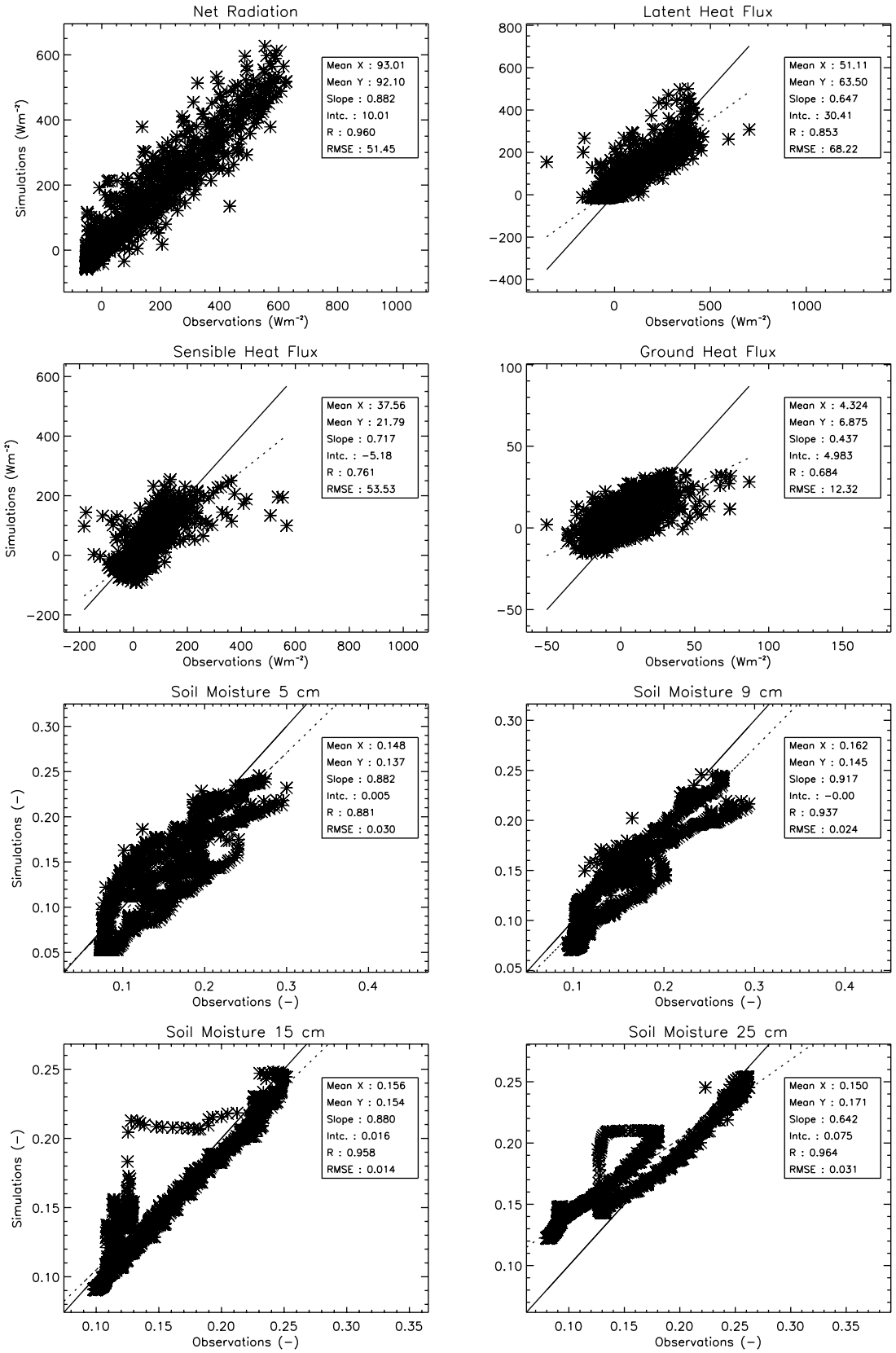

Figure 3. Results of the baseline model calibration. The statistics refer to the linear regressions between the variables on the *x* and *y* axes. Intc. stands for intercept, R stands for correlation coefficient, and RMSE stands for the root-mean-square error.

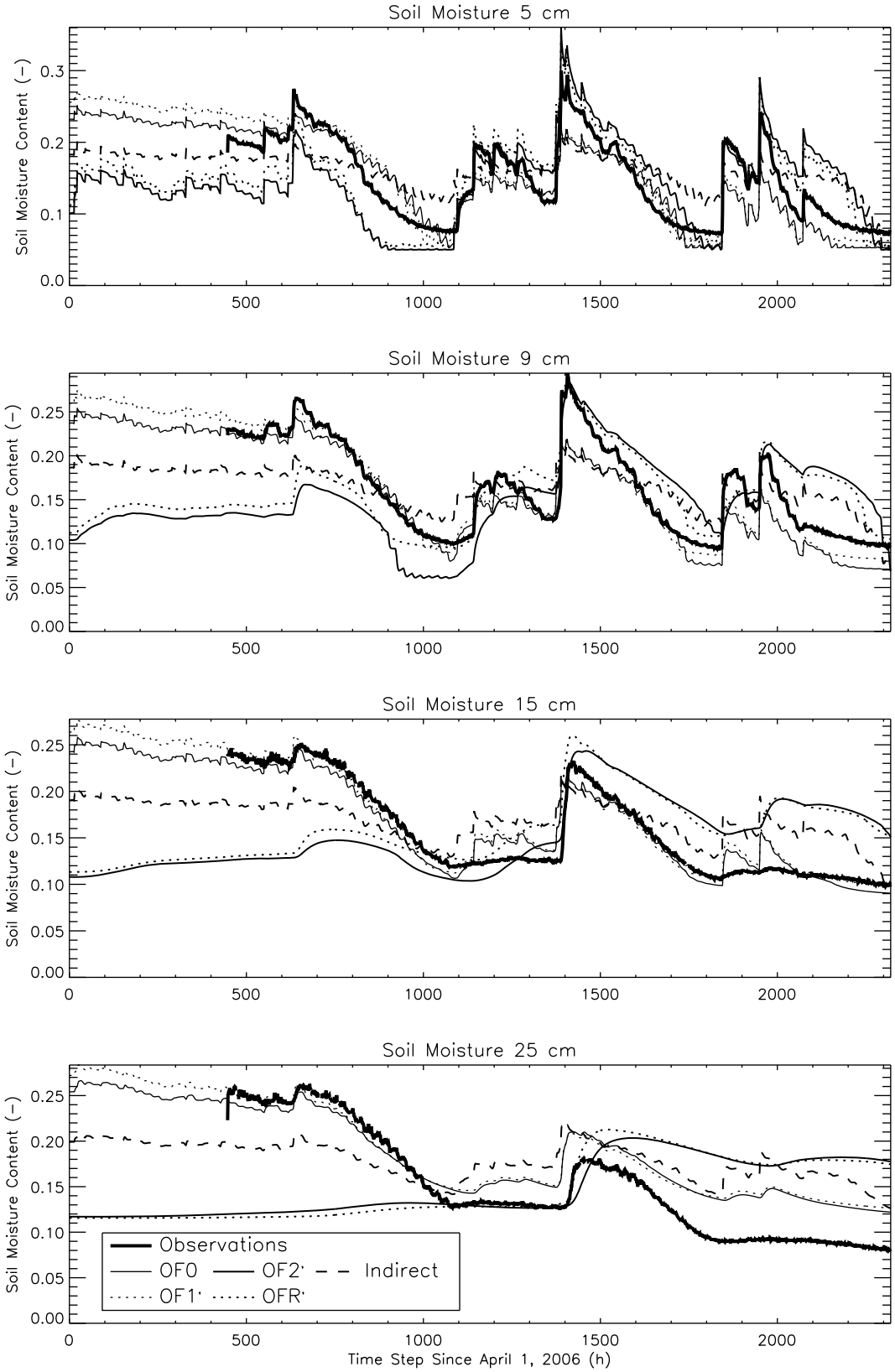

Figure 4. Time series of the modeled soil moisture values, obtained through the minimization of the time domain (OF_0, OF'_R) and the spectral domain (OF'_1, OF'_2) objective functions. The calibration in the spectral domain has also been performed with forcing data that are not overlapping in time with the calibration data (indirect calibration).

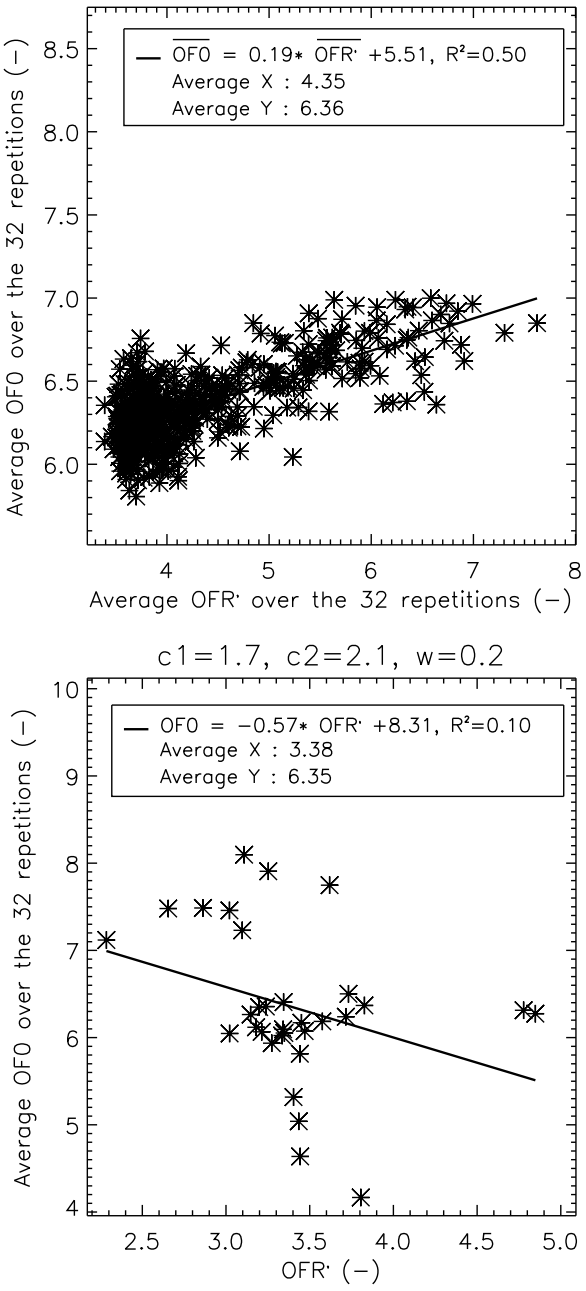

Figure 5. Results of the calibrations on the correlation functions in the time domain. (top) The relationship between the average value for the correlation function objective function and the average corresponding value for OF_0 for all 480 PSO parameter combinations and 32 repetitions for each. (bottom) The relationship between the values for the correlation function objective functions and the corresponding value for OF_0 for the 32 repetitions of the best PSO parameter combination. The PSO parameter values are listed at the top of the plot.

energy balance variables and the observations. Table 4 shows these same statistics for the soil moisture profile variables. Tables 3 and 4 show that the poor model performance in the time domain can be explained by poor model results for both the energy balance terms and the soil moisture profile, except for the the ground heat flux, which is a variable that is modeled well in all cases. This is confirmed by the results in Figure 4, where a poor match of the soil moisture observations can be observed. The different initial values for the soil moisture simulations are caused by the different model parameters. As stated in section 3, equation (1) is solved for the pressure head. Initial hydrostatic conditions are assumed, with an initial water table depth of 2 m. The parameters for the Brooks-Corey equations (ψ_c and λ) are used to convert the modeled pressure head to volumetric soil moisture values. Since the different objective functions result in different parameter values, different initial soil moisture values can result.

[41] The conclusion from the calibration on the correlation functions in the time domain is that this does not lead to a good model performance. It should thus be investigated

Table 2. Value of OF_0 Corresponding to the Model Parameter Set Leading to the Lowest Objective Function Value Within the 32 Repetitions With the Optimal PSO Parameter Set

Objective Function	OF_0 Value
OF'_R	7.12
OF'_1	4.02
OF'_2	7.11
OF'_{1+}	4.14
OF'_{1++}	4.08
Ind[a]	5.35

[a]Ind stands for indirect calibration using OF'_1.

Table 3. Statistics of the Model Energy Balance Results Corresponding to the Lowest Objective Function Value for the Optimal PSO Parameter Set[a]

Statistic	OF_0	OF'_R	OF'_1	OF'_2	OF'_{1+}	OF'_{1++}	Ind
			Net Radiation				
Bias	0.91	35.20	−14.84	36.27	−3.33	−4.98	18.74
Slope	0.88	0.68	0.97	0.64	0.88	0.89	0.77
Intercept	10.01	−5.29	17.66	−2.59	14.69	14.99	2.87
R	0.96	0.96	0.96	0.96	0.96	0.96	0.96
RMSE	51.46	77.20	53.67	82.82	51.58	51.52	62.10
			Latent Heat Flux				
Bias	−12.39	29.62	−19.58	25.38	−5.00	−10.40	−5.12
Slope	0.65	0.21	0.74	0.29	0.61	0.67	0.59
Intercept	30.42	10.79	32.89	11.00	24.88	27.41	26.21
R	0.85	0.81	0.87	0.86	0.87	0.88	0.85
RMSE	68.22	106.02	65.43	96.11	65.58	63.65	69.71
			Sensible Heat Flux				
Bias	15.78	6.88	7.29	11.84	1.75	5.69	25.31
Slope	0.72	0.91	0.73	0.72	0.74	0.70	0.59
Intercept	−5.18	−3.33	2.82	−1.22	7.99	5.76	−10.08
R	0.76	0.74	0.75	0.74	0.74	0.74	0.76
RMSE	53.53	63.01	52.98	55.38	55.11	53.15	55.36
			Ground Heat Flux				
Bias	−2.55	−1.42	−2.61	−0.98	−0.12	−0.31	−1.52
Slope	0.44	0.37	0.43	0.36	0.28	0.29	0.39
Intercept	4.98	4.15	5.06	3.73	3.23	3.36	4.18
R	0.68	0.69	0.68	0.68	0.67	0.68	0.68
RMSE	12.32	12.30	12.36	12.36	12.92	12.79	12.36

[a]The statistics are in W m^{-2}. Bias is defined as the mean of the observations minus the mean of the model simulations. Ind stands for indirect calibration using OF'_1.

Table 4. Statistics of the Model Soil moisture Results Corresponding to the Lowest Objective Function Value for the Optimal PSO Parameter Set[a]

Statistic	OF_0	OF'_R	OF'_1	OF'_2	OF'_{1+}	OF'_{1++}	Ind
			Soil Moisture 5 cm				
Bias	0.012	−0.001	0.007	0.003	0.007	0.008	−0.007
Slope	0.88	0.63	0.94	0.77	0.84	0.90	0.37
Intercept	0.006	0.055	0.001	0.032	0.017	0.006	0.101
R	0.88	0.69	0.89	0.70	0.88	0.87	0.82
RMSE	0.030	0.044	0.029	0.047	0.029	0.030	0.039
			Soil Moisture 9 cm				
Bias	0.016	0.002	0.012	0.009	0.013	0.014	0.002
Slope	0.92	0.33	0.95	0.42	0.92	0.97	0.38
Intercept	−0.003	0.107	−0.003	0.085	0.001	−0.009	0.099
R	0.94	0.45	0.94	0.45	0.94	0.93	0.85
RMSE	0.024	0.048	0.022	0.054	0.022	0.024	0.035
			Soil Moisture 15 cm				
Bias	0.002	−0.007	−0.002	−0.002	−0.002	−0.001	−0.008
Slope	0.88	−0.04	0.91	0.00	0.89	0.95	0.31
Intercept	0.017	0.169	0.017	0.158	0.018	0.008	0.115
R	0.96	−0.06	0.95	0.00	0.95	0.96	0.73
RMSE	0.014	0.060	0.015	0.062	0.015	0.014	0.038
			Soil Moisture 25 cm				
Bias	−0.022	−0.004	−0.024	−0.004	−0.028	−0.027	−0.023
Slope	0.64	−0.36	0.67	−0.32	0.66	0.70	0.22
Intercept	0.075	0.208	0.074	0.203	0.079	0.071	0.140
R	0.96	−0.61	0.96	−0.61	0.95	0.97	0.66
RMSE	0.031	0.082	0.032	0.079	0.036	0.033	0.052

[a]The statistics are dimensionless. Bias is defined as the mean of the observations minus the mean of the model simulations. Ind stands for indirect calibration using OF'_1.

whether a transformation of these functions into the spectral domain, and the use of the spectral properties in the model parameter estimation, leads to a better model performance.

10. Results: Calibration in the Spectral Domain

10.1. Calibration of the Basic Spectral Objective Functions

[42] As in section 9.2, in order to find the optimal PSO parameters for the two basic spectral objective functions (OF'_1 and OF'_2), the values for c_1, c_2 and w were varied with steps of 0.1 within the limits as described in section 8. Again, for each of these PSO parameter combinations the calibration algorithm was repeated 32 times, each time with different initial model parameter values, and the spectral objective function was minimized. With the obtained model parameters, the model was applied, and the corresponding value for OF_0 was calculated for model verification.

[43] Figure 6 (top) shows the relationship between the average values of the basic spectral objective functions and the corresponding average value for OF_0, for each of the 480 PSO parameter combinations, calculated over the 32 repetitions. On average, minimization of OF'_1 leads to a better model performance in the time domain than a minimization of OF'_2. However, for both spectral objective functions, a better fit in the spectral domain tends to lead to a better fit in the time domain. For OF'_1 this relationship is slightly stronger, which is expressed by the higher determination coefficient (R^2) value.

[44] Figure 6 (bottom) shows, for the PSO parameter combination leading to the lowest average value of the basic spectral objective functions, the relationship between this spectral objective function value and the corresponding value of OF_0 for each of the 32 repetitions of the parameter estimation procedure. A conclusion that can be drawn from Figure 6 and Table 2 is that only a minimization of OF'_1 consistently leads to relatively low value for OF_0. For the other basic spectral objective function this is not the case.

[45] A first conclusion that can be drawn from Tables 3 and 4 is that a minimization of OF'_2 tends to lead, for the modeled soil moisture profile, to a lower bias than a minimization of OF'_1 and even a minimization of OF_0. This can be explained by the fact that a similar difference between two $\sqrt{S'}$ values will produce a higher OF'_2 value for large values for $\sqrt{S'}$, while this is not the case for OF'_1. OF'_2 thus emphasizes the larger magnitudes in the Fourier spectrum. For the soil moisture data, Figure 2 shows that these larger amplitudes occur for the first harmonic ($k = 0$). This harmonic corresponds to the average of the time series. It can thus be expected that a minimization of OF'_2 will, for the soil moisture data, focus on a minimization of the bias between the observations and the model simulations. As a consequence, the shape of the time series will be less well matched, which is expressed by the lower slopes, higher intercepts, lower correlation coefficients, and higher RMSE values. This can also be seen in Figure 4, where it can clearly be seen that the dynamics of the soil moisture data are not well matched by the model results obtained from a minimization of OF'_2. Figure 2 also shows that the difference in magnitude between the first harmonic and the rest of the spectrum is not as pronounced for the energy balance data as for the soil moisture data. Consequently, a minimization of OF'_2 does not tend to lead to a lower bias than a minimization of the other objective functions. The relatively high weight of the bias in the soil moisture data in OF'_2 also leads, in general, to a worse model performance in the time domain than a minimization of OF_0.

[46] The fact that OF'_1 puts less emphasis on the larger magnitudes in the Fourier spectrum than OF'_2 can also be seen in the results in Tables 3 and 4. For the soil moisture data, the bias is similar as obtained through a minimization of OF_0, but the fit of the time series tends to be better (regression lines closer to the 1:1 line and similar correlation coefficients and RMSE values). For the energy balance data, the bias in the net radiation and latent heat flux (the major component of the energy balance) tends to be higher through a minimization of OF'_1 as compared to the results obtained through a minimization of OF_0. However, the fit of the time series is better matched. This is expressed by the slopes of the regression lines, which are closer to the 1:1 line. The correlation coefficients and RMSE values are similar in both cases. For the ground heat flux the results are similar for time domain and spectral domain calibration, while for the sensible heat flux the bias is lower for spectral domain calibration. For the sensible heat flux, the other statistics are similar.

[47] Table 5 shows the statistics of the parameter values obtained through 32 repetitions of the calibration algorithm, minimizing OF_0, OF'_1 and OF'_2, for the PSO parameter set leading to the lowest objective function value. A first conclusion that can be drawn from Table 5 is that the standard deviation of the model parameters tends to be relatively large, in some case more than half the parameter value. For both OF_0 and OF'_1, this indicates that similar model statistics

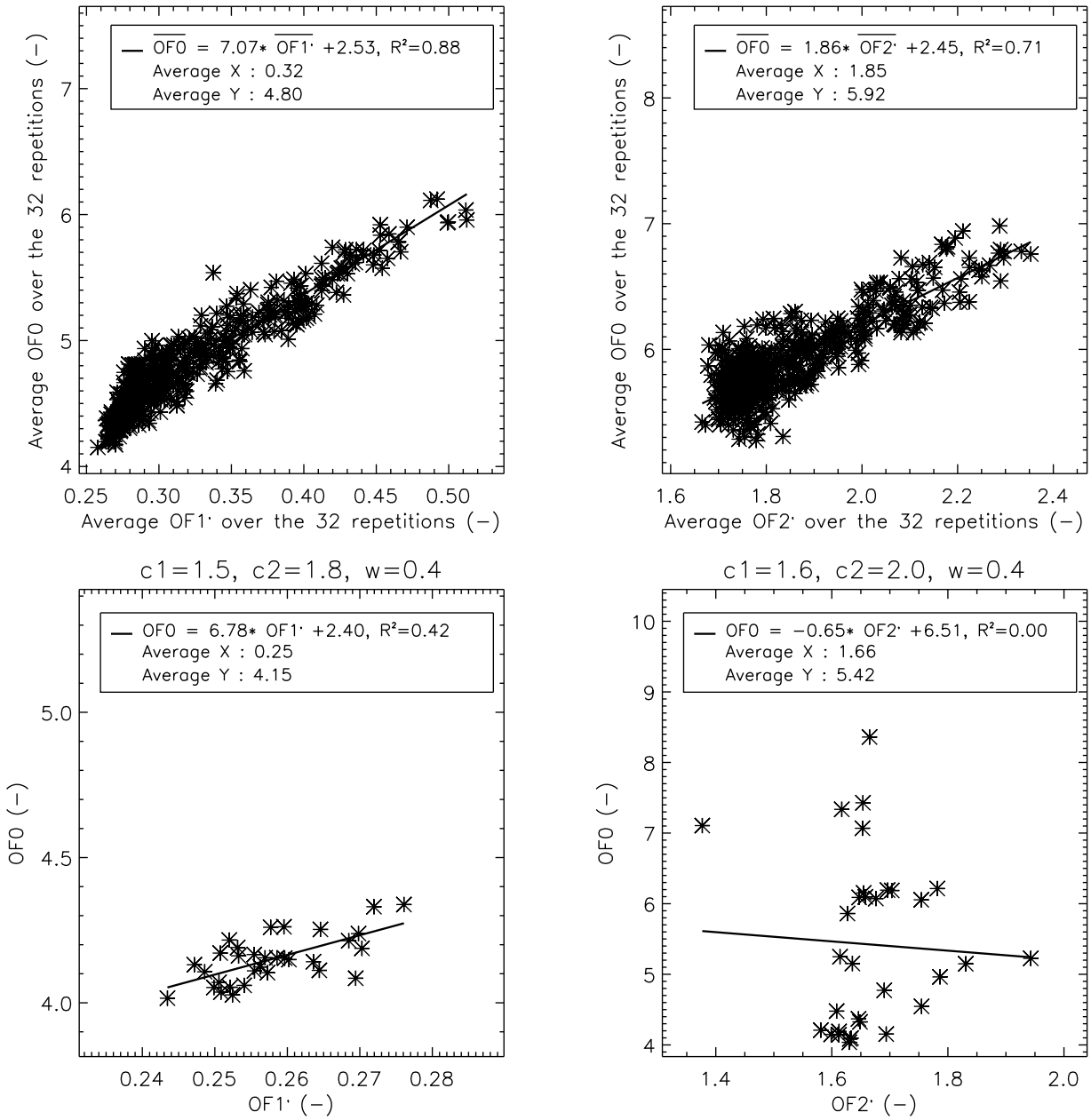

Figure 6. Results of the calibrations on the basic spectral objective functions. (top) The relationship between the average value for the spectral objective function and the average corresponding value for OF_0 for all 480 PSO parameter combinations and 32 repetitions for each. (bottom) The relationship between the values for the spectral objective functions and the corresponding value for OF_0 for the 32 repetitions of the best PSO parameter combination. The PSO parameter values are listed at the top of each plot.

(RMSE values) are obtained with relatively different model parameter sets, a well-known property of nonlinear models referred to as equifinality [*Beven and Binley*, 1992]. Further, Tables 3 and 4 show that, in almost all cases, the difference between the statistics for OF_0 and OF_1' is smaller than the difference between the statistics for OF_0 and OF_2'. Related to this, the model parameters obtained using OF_1' tend to be closer to the model parameters obtained using OF_0 than the model parameters obtained using OF_2'. For OF_2', the sensible and ground heat fluxs are modeled with a similar RMSE as for OF_0, but the net radiation, latent heat flux, and the soil moisture profile have higher RMSE values. For the soil moisture, this can be explained by the strong difference in the parameters related to the drainage of soil water (the top four parameters in Table 5). However, the parameters related to the ground heat flux (κ and C) and sensible heat flux (f_d and f_h) are relatively similar, while the other energy balance parameters tend to be more different.

[48] It can thus be stated that calibration in the spectral domain focuses on different properties of the time series than calibration in the time domain. Depending on the spectral objective function used, similar RMSE values as for time domain calibration can be obtained, but these can be obtained in rather different manners. Depending on the

Table 5. Statistics of the Model Parameters Obtained Through 32 Repetitions of the Minimization of the Time Series and Basic Spectral Objective Functions for the PSO Parameter Combination Leading to the Lowest Average Objective Function Value

Parameter	Units	OF_0	OF'_1	OF'_2
λ		1.02 ± 0.44	0.92 ± 0.24	1.13 ± 0.46
ψ_c	m	−0.87 ± 0.22	−0.93 ± 0.17	−0.68 ± 0.27
K_s	mm h^{-1}	125.73 ± 51.91	151.53 ± 40.61	155.90 ± 69.69
f	m^{-1}	13.98 ± 2.63	16.22 ± 1.72	7.30 ± 5.35
α		0.09 ± 0.04	0.04 ± 0.03	0.15 ± 0.13
κ	W m^{-1} K^{-1}	0.08 ± 0.01	0.09 ± 0.02	0.08 ± 0.02
C	J m^{-3} K^{-1}	226,933.38 ± 39,823.23	224,642.55 ± 44,793.05	225,662.72 ± 43,916.31
r_c	s m^{-1}	103.86 ± 33.27	102.89 ± 33.23	130.56 ± 60.03
f_d		0.60 ± 0.12	0.59 ± 0.14	0.55 ± 0.13
f_h		0.18 ± 0.06	0.22 ± 0.09	0.15 ± 0.13
f_v		0.29 ± 0.14	0.34 ± 0.10	0.25 ± 0.16

shape of the Fourier spectrum, better fits of the time series can be obtained in a combination with worse bias values, or vice versa.

[49] There is thus certainly a benefit in transforming the calculated correlation functions to the spectral domain. This can be explained by the properties of these functions. Correlation functions will focus on the way modeled variables are autocorrelated in time. A good autocorrelation in time can be achieved by a poor match of other properties. On the other hand, calibration on the spectral properties of a time series focuses on different properties of the time series. Each individual harmonic represents a wave with a specific periodicity. Focusing on the spectral properties will thus attempt to match all these different waves. A match of all the different waves represented by the spectral densities can thus be expected to lead to an overall decent match of the time series in the time domain. In other words, calibrating on the spectral properties uses the information from the correlation functions in a more efficient way.

[50] On the basis of the results in this section, it can be concluded that multivariate model calibration in the spectral domain is best performed by matching the square roots of the spectral densities (thus by matching the amplitudes of the waves in the time domain).

10.2. Incorporation of the Cross Spectra in the Spectral Objective Functions

[51] As stated in section 5.4, an interesting aspect in spectral calibration is the possibility to include information on the cross correlation between different variables. Since it has already been shown that it is best to match the square roots of the spectral densities, this section will focus on the results obtained using OF'_{1+} (equation (21)) and OF'_{1++} (equation (22)). Figure 7 (top) shows the relationship between the average value for the extended spectral objective functions and the average corresponding value for OF_0, for each of the 480 PSO parameter combinations. Similar to OF'_1, a strong relationship can be seen, with on average a slightly lower value for OF_0, as compared to the results obtained from a minimization of OF'_1. Figure 7 (bottom) shows, for the PSO parameter combination leading to the lowest average value for the extended spectral objective function, the relationship between the spectral objective function values and the corresponding value for OF_0, for each of the 32 repetitions. Again, a strong correlation can be seen, however, with a slightly higher average value for OF_0, as compared to the results obtained from a minimization of OF'_1. Table 2 shows that the lowest extended spectral objective function value corresponds to a value for OF_0 that is slightly higher than the result for the minimization of OF'_1. Tables 3 and 4 show that for all variables similar results are obtained as through the minimization of OF'_1. From these results, it can be concluded that there is not a real benefit in using information on the cross correlation in the model calibration. This can be explained by the aggregation of the objective functions for the different variables into the basic spectral objective functions. Through this aggregation, one could argue that the cross correlation between the different variables is implicitly included in the calibration. Explicitly including the cross correlation thus means that the same information is included twice in the calibration, which will thus not improve the results.

10.3. Application With Nonoverlapping Meteorological Forcing and Calibration Data

[52] An interesting application of calibrating models in the spectral domain is the possibility to estimate the model parameters if the meteorological forcing data and the model calibration data are not overlapping in time [*Montanari and Toth*, 2007]. In order to assess whether this can also be performed when multiple variables are used to estimate the model parameters, the following experiment was performed. Instead of using both the meteorological forcings and model calibration data from 1 April through 5 July 2006, as is performed in all model simulations described above, forcings were taken from exactly the same period in 2005. Thus, the model was forced with meteorological data from 1 April through 5 July 2005, while it was calibrated using energy balance and soil moisture profile observations from 1 April through 5 July 2006. On the basis of the results in section 10.1, OF'_1 was used as objective function. Again, the calibration algorithm was repeated 32 times, and the model parameter set leading to the lowest value for OF'_1 was retained. The meteorological data from 1 April through 5 July 2006 were then used to force the model, and the resulting energy balance terms and soil moisture profiles were contrasted to the observations. The results from this latter model application are referred to as the results from the indirect calibration.

[53] Table 2 shows that the value for OF_0 from this indirect calibration is slightly higher than the result from the direct calibration. Table 3 shows that the RMSE for the net radiation is slightly higher for the indirect calibration, while for the three fluxes the results are rather similar. Table 4

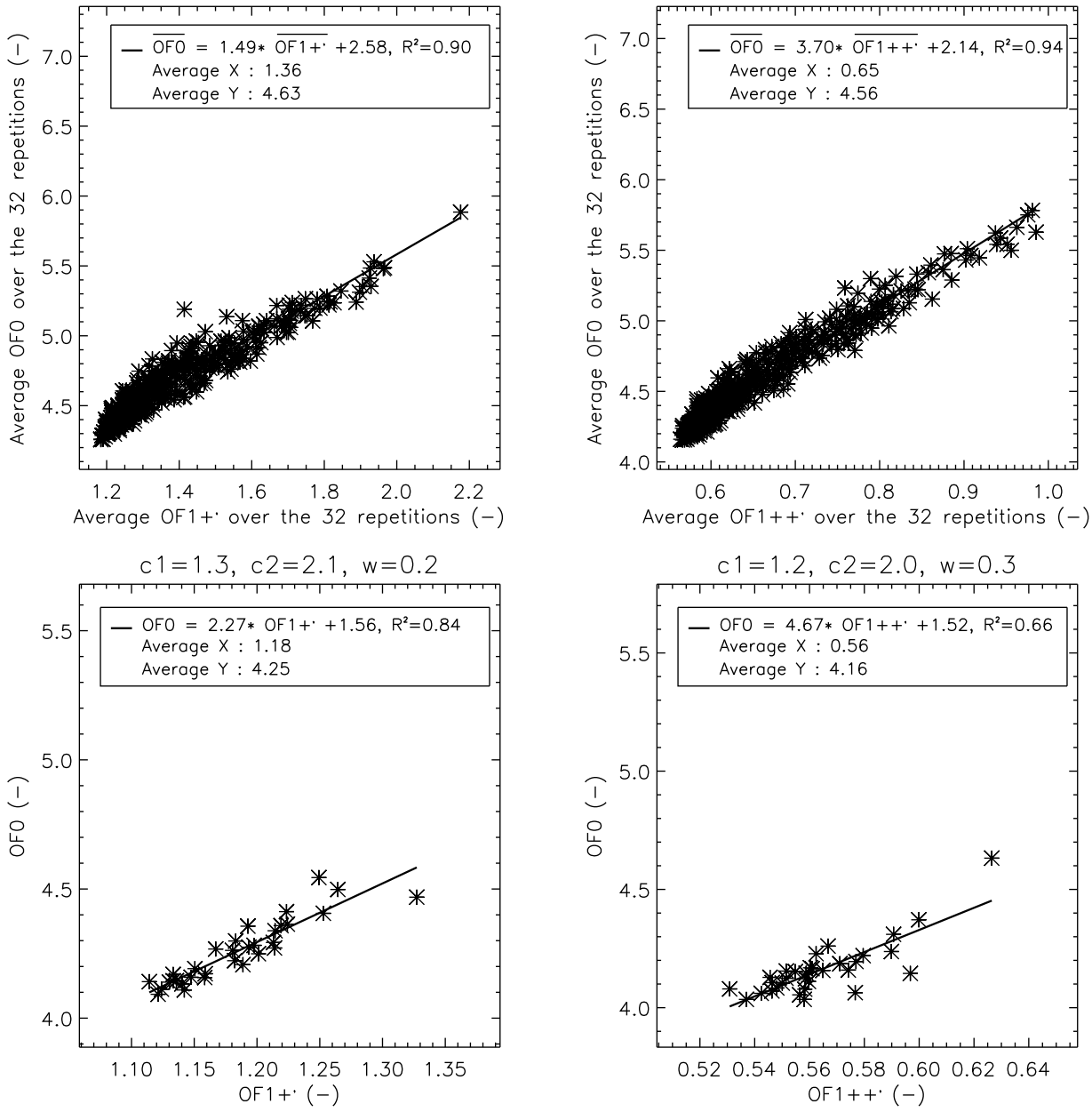

Figure 7. Results of the calibrations on the extended spectral objective functions. (top) The relationship between the average value for the extended spectral objective function and the average corresponding value for OF_0 for all 480 PSO parameter combinations and 32 repetitions for each. (bottom) The relationship between the values for the spectral objective functions and the corresponding value for OF_0 for the 32 repetitions of the best PSO parameter combination. The PSO parameter values are listed at the top of each plot.

shows that the error in the modeled soil moisture is slightly higher for all levels if indirect calibration is performed. Figure 4 compares the temporal evolution of the modeled soil moisture to the observations. From Table 4 and Figure 4 it can be concluded that both the bias and the temporal evolution are better if direct calibration is performed, but that indirect calibration does lead to an acceptable match of the observations.

[54] A conclusion from this model application is that there is a possibility to use nonoverlapping data for model calibration using multiple variables. Even though, as can be expected, the model performance is not as good as for direct calibration, an acceptable model performance can result from this strategy.

10.4. Separate Calibration and Validation Periods

[55] In order to divide the data set into a training data set and a validation data set, the approach of *Scheerlinck et al.* [2009] was used, in which the simulation period was divided into two periods. The first period contains the BREB and TDR measurements from 20 April through 21 June, whereas the second period contains data measured from 22 June

Table 6. Results of the Model Application During the Validation Period for the Calibration With a Separate Calibration and Validation Period

Objective Function	Units	Mean Observations	Mean Simulations	Slope	Intercept	R	RMSE
			Net Radiation				
OF_0	W m^{-2}	123.08	125.01	0.87	17.86	0.96	55.75
OF_1'	W m^{-2}	123.08	145.49	0.98	24.92	0.96	59.11
			Latent Heat Flux				
OF_0	W m^{-2}	74.26	90.22	0.80	30.64	0.88	67.40
OF_1'	W m^{-2}	74.26	106.10	0.92	37.61	0.88	76.63
			Sensible Heat Flux				
OF_0	W m^{-2}	43.88	17.99	0.49	−3.43	0.81	60.44
OF_1'	W m^{-2}	43.88	18.65	0.52	−4.04	0.80	59.52
			Ground Heat Flux				
OF_0	W m^{-2}	4.93	16.87	0.74	13.21	0.72	16.32
OF_1'	W m^{-2}	4.93	20.82	0.89	16.43	0.72	20.33
			Soil Moisture 5 cm				
OF_0		0.12	0.10	0.87	−0.00	0.88	0.029
OF_1'		0.12	0.09	0.73	0.01	0.91	0.032
			Soil Moisture 9 cm				
OF_0		0.13	0.12	0.90	−0.00	0.95	0.018
OF_1'		0.13	0.11	0.74	0.01	0.96	0.025
			Soil Moisture 15 cm				
OF_0		0.12	0.14	0.87	0.03	0.91	0.017
OF_1'		0.12	0.13	0.62	0.05	0.82	0.016
			Soil Moisture 25 cm				
OF_0		0.11	0.16	0.63	0.10	0.98	0.057
OF_1'		0.11	0.15	0.47	0.10	0.97	0.050

through 5 July. When taking into account the missing data points, both periods contain approximately 50% of the available BREB and TDR data. The first period is used to estimate the model parameters, while the second period is used for model validation. Since the results from the previous indicate that for calibration in the spectral domain OF_1' leads to the best results, this objective function was used for this purpose. Again, the calibration algorithm was repeated 32 times, with the PSO parameters determined in section 9.1 for OF_0 and section 10.1 for OF_1'. The model parameter set leading to the lowest objective function value was retained, and using these model parameters the model was applied. The BREB and TDR measurements from 22 June through 5 July were then used to validate the model results.

[56] For the calibration on OF_0, the lowest objective function obtained was 3.83. For OF_1' the lowest value obtained was 0.19, which corresponds to a value of 4.02 for OF_0. Table 6 shows the results of the model application during the validation period. The same conclusions can be drawn as for the results in Tables 3 and 4. More specifically, OF_1' leads to a slightly higher RMSE than OF_0 for the energy balance data, but the slopes of the regression lines are closer to the 1:1 line. For the soil moisture data, the RMSE values for the first and third layer are similar for both objective functions. However, for the second layer OF_0 leads to better results, while for the fourth layer the results obtained from OF_1' have a slightly lower RMSE. Overall, the results from Table 6 indicate that when a separate model validation during a different period is performed, calibration in the spectral domain leads to an almost equal model performance as calibration in the time domain.

11. Discussion and Conclusions

[57] In this paper, the possibility to perform model calibration in the spectral domain using observations from multiple variables has been explored. A simple water and energy balance model has been used for this purpose, and particle swarm optimization has been used as calibration algorithm. The spectral density functions of the time series have been calculated through a Fourier transform of the correlation functions for the different variables. These spectral coefficients were then used in the parameter estimation procedure. It is best to use the square roots of the spectral densities in the parameter estimation. Under these conditions, the resulting parameters led to an almost equal model performance in the time domain as time domain calibration using the RMSE between the untransformed time series. Calibration on the correlation functions without transformation into the spectral domain resulted in a worse model performance in the time domain. This can be explained by the matching of the individual waves in the time series for spectral calibration, instead of the fitting of the correlation with different lags if calibration is performed on the correlation functions directly. Incorporation of information on the cross spectra between the different calibration variables did not improve the results. An indirect calibration has then been performed, in which the meteorological forcing data and the calibration data were not overlapping in time. This

has been found to lead to an acceptable model performance which was, as expected, slightly worse then for direct calibration. In this paper, only simple, quadratic objective functions were used in the optimization algorithm. Future research could focus on the use of more complex functions, such as the Whittle likelihood, and on an evaluation of the assumptions of these objective functions [*Feyen et al.*, 2007; *Thyer et al.*, 2009; *Schoups and Vrugt*, 2010]. Overall, the results in this paper suggest that there is a possibility to use spectral calibration techniques for model calibration using multiple variables, if the different data sets required for this purpose are available at different times.

[58] **Acknowledgments.** The second author is a postdoctoral researcher funded by the Foundation for Scientific Research of the Flemish Community (FWO-Vlaanderen). We would like to thank Davy Loete, Alexander Loew, and Ingo Keding for their help with the installation and maintenance of the Bowen ratio and soil moisture stations, Edgar Zabel for maintaining the Bowen ratio station between the field campaigns, and the entire AgriSAR team for their help with the collection of the various in situ data sets. We would also like to thank the Foundation for Scientific Research of the Flemish Community (FWO-Vlaanderen) for their funding of the Bowen Ratio equipment. Computational resources and services used in this work were provided by Ghent University.

References

Beven, K., and A. Binley (1992), The future of distributed models: Model calibration and uncertainty prediction, *Hydrol. Processes*, *6*(3), 279–298.

Beven, K. J., and M. J. Kirkby (1979), A physically based, variable contributing area model of basin hydrology, *Hydrol. Sci. Bull.*, *24*(1), 43–69.

Box, G. E. P., and G. M. Jenkins (1970), *Time Series Analysis, Forecasting and Control*, Holden-Day, San Francisco, Calif.

Brooks, R. H., and A. T. Corey (1964), Hydraulic properties of porous media, *Hydrol. Pap. 3*, Colo. State Univ., Fort Collins.

Brown, R. G., and P. Y. C. Hwang (1992), *Introduction to Random Signals and Applied Kalman Filtering*, John Wiley, London.

Castagna, M., and A. Bellin (2009), A Bayesian approach for inversion of hydraulic tomographic data, *Water Resour. Res.*, *45*, W04410, doi:10.1029/2008WR007078.

Clerc, M. (2006), *Particle Swarm Optimization*, ISTE, London.

Crow, W. T., E. F. Wood, and M. Pan (2003), Multiobjective calibration of land surface model evapotranspiration predictions using streamflow observations and spaceborne surface radiometric temperature retrievals, *J. Geophys. Res.*, *108*(D23), 4725, doi:10.1029/2002JD003292.

Duan, Q., S. Sorooshian, and V. Gupta (1992), Effective and efficient global optimization for conceptual rainfall-runoff models, *Water Resour. Res.*, *28*(4), 1015–1031.

Duan, Q. Y., S. Sorooshian, and V. K. Gupta (1994), Optimal use of the SCE-UA global optimization method for calibrating watershed models, *J. Hydrol.*, *158*(3–4), 265–284.

Engelbrecht, A. (2003), *Fundamentals of Computational Swarm Intelligence*, John Wiley, London.

Fenicia, F., J. J. McDonnell, and H. H. G. Savenije (2008), Learning from model improvement: On the contribution of complementary data to process understanding, *Water Resour. Res.*, *44*, W06419, doi:10.1029/2007WR006386.

Feyen, L., J. A. Vrugt, O. Naullain, J. van der Knijff, and A. De Roo (2007), Parameter optimization and uncertainty assessment for large-scale streamflow simulation with the LISFLOOD model, *J. Hydrol.*, *332*(3–4), 276–289.

Gan, T. Y., and G. F. Biftu (1996), Automatic calibration of conceptual rainfall-runoff models: Optimization algorithms, catchment conditions, and model structure, *Water Resour. Res.*, *32*(12), 3513–3524.

Gill, M. K., Y. H. Khalil, M. McKee, and L. Bastidas (2006), Multiobjective particle swarm optimization for parameter estimation in hydrology, *Water Resour. Res.*, *42*, W07417, doi:10.1029/2005WR004528.

Gupta, H. V., L. A. Bastidas, S. Sorooshian, W. J. Shuttleworth, and Z. L. Wang (1999), Parameter estimation of a land surface scheme using multicriteria methods, *J. Geophys. Res.*, *104*(D16), 19,491–19,503.

Houser, P. R., H. V. Gupta, W. J. Shuttleworth, and J. Famiglietti (2001), Multiobjective calibration and sensitivity of a distributed land surface water and energy balance model, *J. Geophys. Res.*, *106*(D24), 33,421–33,433.

Kennedy, J., and R. C. Eberhart (1995), Particle swarm optimization, in *1995 IEEE International Conference on Neural Networks: Proceedings*, pp. 1942–1949, IEEE Press, Piscataway, N. J.

Liu, J., and D. Han (2010), Indices for calibration data selection of the rainfall-runoff model, *Water Resour. Res.*, *46*, W04512, doi:10.1029/2009WR008668.

Madsen, H. (2003), Parameter estimation in distributed hydrological catchment modelling using automatic calibration with multiple objectives, *Adv. Water Resour.*, *26*(2), 205–216.

Montanari, A., and E. Toth (2007), Calibration of hydrological models in the spectral domain, an opportunity for scarcely gauged basins?, *Water Resour. Res.*, *43*, W05434, doi:10.1029/2006WR005184.

Mousavi, S. J., and M. Shourian (2010), Adaptive sequentially space-filling metamodeling applied in optimal water quantity allocation at basin scale, *Water Resour. Res.*, *46*, W03520, doi:10.1029/2008WR007076.

Papoulis, A. (1965), *Probability, Random Variables and Stochastic Processes*, McGraw-Hill, New York.

Pauwels, V. R. N., W. Timmermans, and A. Loew (2008), Comparison of the estimated water and energy budgets of a large winter wheat field during AgriSAR 2006 by multiple sensors and models, *J. Hydrol.*, *349*(3–4), 425–440.

Quets, J. J., G. J. M. De Lannoy, and V. R. N. Pauwels (2010), Comparison of spectral and time domain calibration methods for precipitation-discharge processes, *Hydrol. Processes*, *24*(8), 1048–1062.

Reed, P., B. Minsker, and D. Goldberg (2000), Designing a competent simple genetic algorithm for search and optimization, *Water Resour. Res.*, *36*(12), 3757–3761.

Reed, P., B. S. Minsker, and D. E. Goldberg (2003), Simplifying multiobjective optimization: An automated design methodology for the nondominated sorted genetic algorithm-II, *Water Resour. Res.*, *39*(7), 1196, doi:10.1029/2002WR001483.

Richards, L. (1931), Capillary conduction of liquids through porous media, *Physics*, *1*(1), 318–333.

Scheerlinck, K., V. R. N. Pauwels, H. Vernieuwe, and B. De Baets (2009), Calibration of a water and energy balance model: Recursive parameter estimation versus particle swarm optimization, *Water Resour. Res.*, *45*, W10422, doi:10.1029/2009WR008051.

Schoups, G., and J. A. Vrugt (2010), A formal likelihood function for parameter and predictive inference of hydrologic models with correlated, heteroscedastic and non-Gaussian errors, *Water Resour. Res.*, *46*, W10531, doi:10.1029/2009WR008933.

Shuttleworth, W. J. (1992), Evapotranspiration, in *Evaporation*, pp. 4.1–4.53, McGraw-Hill, New York.

Sivapalan, M., et al. (2003), IAHS science decade on prediction in ungauged basins (PUB), 2003–2012: Shaping an exciting future for the hydrological sciences, *Hydrol. Sci. J.*, *48*(6), 857–880.

Thiemann, M., M. Trosset, H. Gupta, and S. Sorooshian (2001), Bayesian recursive parameter estimation for hydrologic models, *Water Resour. Res.*, *37*(10), 2521–2536, doi:10.1029/2000WR900405.

Thyer, M., G. Kuczera, and B. C. Bates (1999), Probabilistic optimization for conceptual rainfall-runoff models: A comparison of the shuffled complex evolution and simulated annealing algorithms, *Water Resour. Res.*, *35*(3), 767–773.

Thyer, M., B. Renard, D. Kavetski, G. Kuczera, S. W. Franks, and S. Srikanthan (2009), Critical evaluation of parameter consistency and predictive uncertainty in hydrological modeling: A case study using Bayesian total error analysis, *Water Resour. Res.*, *45*, W00B14, doi:10.1029/2008WR006825.

Tolson, B. A., and C. A. Shoemaker (2007), Dynamically dimensioned search algorithm for computationally efficient watershed model calibration, *Water Resour. Res.*, *43*, W01413, doi:10.1029/2005WR004723.

Tolson, B. A., and C. A. Shoemaker (2008), Efficient prediction uncertainty approximation in the calibration of environmental simulation models, *Water Resour. Res.*, *44*, W04411, doi:10.1029/2007WR005869.

Tolson, B. A., M. Asadzadeh, H. R. Maier, and A. Zecchin (2009), Hybrid discrete dynamically dimensioned search (HD-DDS) algorithm for water distribution system design optimization, *Water Resour. Res.*, *45*, W12416, doi:10.1029/2008WR007673.

Trelea, I. C. (2003), The particle swarm optimization algorithm: Convergence analysis and parameter selection, *Inf. Process. Lett.*, *85*(6), 317–325.

Vrugt, J. A., H. V. Gupta, L. A. Bastidas, W. Bouten, and S. Soorooshian (2003a), Effective and efficient algorithm for multiobjective optimization of hydrologic models, *Water Resour. Res.*, *39*(8), 1214, doi:10.1029/2002WR001746.

Vrugt, J. A., H. V. Gupta, W. Bouten, and S. Soorooshian (2003b), A shuffled complex evolution Metropolis algorithm for optimization and uncertainty assessment of hydrologic models, *Water Resour. Res.*, *39*(8), 1201, doi:10.1029/2002WR001642.

Winsemius, H. C., B. Schaefli, A. Montanari, and H. H. G. Savenije (2009), On the calibration of hydrological models in ungauged basins: A framework for integrating hard and soft hydrological information, *Water Resour. Res.*, *45*, W12422, doi:10.1029/2009WR007706.

Yapo, P. O., H. V. Gupta, and S. Sorooshian (1998), Multi-objective global optimization for hydrologic models, *J. Hydrol.*, *204*(1–4), 83–97.

Zhang, Y., and F. H. S. Chiew (2010), Relative merits of different methods for runoff predictions in ungauged catchments, *Water Resour. Res.*, *46*, W07412, doi:10.1029/2008WR007504.

G. J. M. De Lannoy and V. R. N. Pauwels, Laboratory of Hydrology and Water Management, Ghent University, Coupure links 653, B-9000 Ghent, Belgium. (Gabrielle.DeLannoy@UGent.be; Valentijn.Pauwels@UGent.be)